

Grid graph convolutional network-cyclical learning rate EfficientNet for liver tumor segmentation classification

Sangi Narasimhulu, Ch D V Subba Rao

Department of Computer Science and Engineering, Sri Venkateswara University College of Engineering, Tirupathi, India

Article Info

Article history:

Received Jan 4, 2025

Revised Jun 29, 2025

Accepted Jul 13, 2025

Keywords:

Computed tomography

Cyclical learning rate

EfficientNet data augmentation

Grid-graph convolutional network

ResNext50

ABSTRACT

Liver tumors are identified in computed tomography (CT) images, which are crucial for accurate disease diagnosis and treatment planning as they enable clear delineation of tumors. Hence, it is vital in the field of medical radiology to segment and classify CT images of liver tumors effectively. However, liver tumor locations are not captured accurately at the boundaries in terms of size and depth within the liver due to downsampled images, leading to reduced segmentation and classification results. This research proposes a grid-graph convolutional network-based cyclical learning rate EfficientNet (GGCN-CLREN) to accurately segment and classify liver tumors. GGCN addresses inaccurate liver tumor segmentation due to downsampled images, which capture spatial relationships effectively and preserve tumor boundaries as well as depth information. For classification, CLREN optimizes classification by adjusting the learning rate, which enhances convergence and accuracy. Therefore, GGCN-CLREN ensures enhanced segmentation and classification by addressing size and depth inaccuracies. Golden sine gray wolf optimization (GSGWO) selects the most appropriate features effectively. The GGCN-CLREN achieves commendable accuracies of 99.80% and 99.96%, respectively, for the LiTS17 and CHAOS datasets when compared to the existing techniques: enhanced swim transformer network with adversarial propagation (APESTNet) and adding inception module-UNet (AIM-UNet).

This is an open access article under the [CC BY-SA](#) license.



Corresponding Author:

Sangi Narasimhulu

Department of Computer Science and Engineering, Sri Venkateswara University College of Engineering
Tirupathi, India

Email: narasimhulu.sangi@gmail.com

1. INTRODUCTION

Liver tumors are one of the primary and lethal forms of cancer all over the world, causing a large number of deaths every year. Primary liver cancers are often caused by cirrhosis, resulting from hepatitis B or C, alcohol consumption, or fatty liver disease [1]. Numerous imaging tests, such as ultrasound, computer tomography (CT), and magnetic resonance imaging (MRI), assist in diagnosing cirrhosis. Among these, CT is the primary method used for diagnosis. CT provides comprehensive cross-sectional abdomen images that enable it, inclusive of all tests [2], [3]. This is because the contrast enhancement in CT images helps distinguish the tumor region from liver parenchyma [4]. Hence, it is significant in the medical radiology field for segmenting CT images of liver tumors accurately [5]. Glycogen storage, regulation of hormone production, and red blood cell (RBC) degradation are various metabolic processes carried out in the liver [6]. Annotating liver tumors from a large number of abdominal images is time-consuming and laborious, requiring medical expertise. Moreover, partial volume effect and low-dose artifacts in medical imaging make it even more challenging to delineate accurate lesion boundaries, resulting in intra-rater variations [7], [8].

Segmentation is essential for post-interventional tracking of ablated liver tissue, as it helps assess negative tissue margins and allows clinicians to evaluate the effectiveness of the process [9]. Additionally, liver tumor segmentation permits structural analyses, like tumor volume estimation, which is significant in follow-up diagnosis, image-driven surgery, and therapy [10]. Accurate segmentation enables the evaluation of volume-based quantitative data, including the textural features, which help in liver therapy planning and generate a more consistent hepatic tumor classification, therapeutic response classification, and patient survival prediction [11]. The categorization of segmentation techniques is often subjective, as they are categorized depending on the extent of human intervention or methodology. The methodology-based classification includes model-based approaches based on statistical shape, active contours, graph cuts, and region growing [12], [13]. Model-based techniques are inclined to achieve better segmentation performance than intensity-based techniques due to their mathematical and accurate statistical modeling that captures the region of interest (RoI) [14], [15]. However, the locations of liver tumors are not accurately captured at the boundaries for size and depth due to downsampled images, further leading to reduced segmentation and classification accuracy. To overcome this issue, grid-graph convolutional network-based cyclical learning rate EfficientNet (GGCN-CLREN) is proposed to accurately segment and classify liver tumors by leveraging graph convolutional network (GCN) and dynamic learning rate adjustments, which ensure accurate delineation and tumor classification.

The main contributions to liver tumor segmentation are explained as follows:

- GGCN learns the structural data by representing the image as a graph, which models the relationships among regions or neighborhood pixels more effectively, leading to accurate segmentation.
- Gray wolf optimization (GWO) integrates the effective exploration capabilities with search diversity enhancement provided by the golden sine strategy, which assists in navigating the search space effectively to identify appropriate features for classification.
- Cyclical learning rate (CLR) adjusts the learning rate dynamically during training, which further increases model convergence and generalization. This approach assists EfficientNet in effectively learning complex features, which improves classification accuracy and robustness. By performing all these processes, the proposed approach achieves better performance in liver tumors.

The research paper is organised as follows: section 2 details the literature review of existing techniques. Section 3 presents detailed information about the proposed methodology. Section 4 analyzes the experimental results of the existing techniques and proposed methodology. Section 5 provides the conclusion of this research paper.

2. LITERATURE SURVEY

The related works of liver tumor segmentation based on CT images are briefly explained in this section, along with their benefits and limitations. These methods improve accuracy by capturing detailed tumor boundaries and leveraging spatial information. As a result, they contribute to improved diagnosis and treatment planning in medical imaging.

Wang *et al.* [16] suggested an EfficientNetB4, attention gate, and residual learning (EAR-UNet) approach to attain automatic and accurate segmentation of liver tumors. Initially, EfficientB4 was performed as the encoder for extracting more features during the encoding phase. Then, an attention gate was applied in the skip connection to remove inappropriate regions and highlight specific regions. At last, decoder convolution in UNet was replaced with a residual block to reduce the vanishing gradient issue, which enhanced the convergence speed. However, EfficientNetB4 struggled to manage heterogeneous tumor textures due to the variability of tumor appearance that challenged the model's ability to generalize effectively.

Di *et al.* [17] implemented an automated approach based on hierarchical iterative superpixels and local statistical features to segment liver tumors. Initially, 3D UNet was used for extracting liver regions, and a hierarchical superpixel approach was applied to detect tumor boundaries accurately. Each pixel in the liver region was then categorized into non-tumor or tumor using a support vector machine (SVM). A Euclidean distance voting approach was employed, which incorporated superpixel segmentation and pixel-wise classification to effectively and automatically identify tumor regions. Nevertheless, this approach did not capture complex spatial relationships and variations within tumors, as it relied on predefined local structures, resulting in inaccurate results.

Manjunath and Kwadiki [18] presented a modified residual UNet (ResUNet) based on a convolutional neural network (CNN) to segment the liver from CT images and lesions from segmented liver portions. In the pre-processing phase, each image was resized, and a normalization technique was applied to every image to obtain a value between zero and one. The presented approach represented the ability to segment the liver accurately by automated tumor segmentation. However, the modified ResUNet struggled with significant inter-patient variability in liver shape and lesion appearance

because its learned features did not generalize well across different pathologies, which resulted in inaccurate segmentation.

Lv *et al.* [19] introduced deep supervision (DS) and atrous inception (AI) with conditional random field (CRF) to segment liver regions. Initially, the encoder's standard convolution was replaced by a residual block, which enhanced the network's depth. Then, the AI approach was applied to interconnect the encoder and decoder blocks, which enabled to obtain the multi-scale features. The CRF was performed to enhance the adjacent data's labeling deviation, which led to the refinement of overall liver boundaries. However, this approach resulted in over or under-segmentation errors for level tumors situated at the boundaries due to their complex spatial relationships and variations.

Popescu *et al.* [20] developed advanced CNN techniques to segment the liver and hepatic tumors by incorporating four effective neural networks like ResNeXt101, ResNet152, DenseNet201, and InceptionV3. Global segmentation was performed by training separate individual classifiers and then integrating its decision into a unified system. The images underwent a post-processing process that effectively removed artifacts after segmentation based on the neural networks. However, the CNN suffered from limited generalization across diverse imaging conditions because of variations in image quality and anatomical differences among patients.

Balasubramanian *et al.* [21] presented an enhanced swim Transformer network with adversarial propagation (APESTNet) to segment and classify liver tumors. Medium filtering and histogram equalization were utilized in the pre-processing phase, which improved the input images. The enhanced mask region CNN (R-CNN) was applied for segmenting the liver tumor, and APESTNet was employed to categorize the liver tumor. Overfitting problems were solved using the swim Transformer model by constructing adversarial propagation in the classifier. However, APESTNet faced challenges in adapting to different tumor appearances and anatomical variations, as a result of capturing subtle features specific to different tumor types.

Kolli *et al.* [22] implemented an improved probabilistic neural network and Bayesian optimization (IPNN-BO) to classify liver tumors. The fully automated approach was used to separate malignancies and the liver from CT scans. Optimal hyperparameter tuning was automatically applied by utilizing BO with IPNN approach, which achieved accurate segmentation and classification results. However, the implemented approach faced struggles with intricate interactions among tumor characteristics due to complex and non-linear relationships among various features.

Özcan *et al.* [23] suggested adding inception module-UNet (AIM-UNet) by integrating UNet and InceptionV3 to segment liver tumors. Data augmentation, image rotation, resizing, and slicing were utilized in the pre-processing stage to increase the dataset size and resize the images. AIM-UNet was developed by placing convolutional layers of various filter sizes on a skip connection. The suggested approach provided better performances by processing edge data and morphology features to a greater extent. However, AIM-UNet suffered from increased memory usage and potential overfitting due to a large number of parameters introduced by Inception modules, which impacted the model's performance.

Xia *et al.* [24] developed a multiview information fusion and CRF to segment liver tumors. Initially, the dual self-attention (DSA) approach was employed to determine the significant spatial structures and patterns, as well as capture relationships among various feature dimensions and channels. A lightweight 3D network was constructed to combine segmentation results from different views and produce a 3D outcome. At last, CRF was generated for 3D segmentation refinement, which eliminated over-segmented errors and enhanced segmentation accuracy. Nevertheless, the developed approach was a pseudo-3D technique that extracted 3D feature data by combining 2D segmentation outcomes from various perspectives, which resulted in the loss of certain subtle patterns.

Xie *et al.* [25] introduced a multi-scale context integration network (MCI-Net) to segment liver images. The residual approach was constructed to avoid network degradation. The multi-scale context extraction module was deployed by integrating hybrid dilated convolutions to capture deeper and broader features at different scales. A boundary correction block was generated, which enhanced the localization capability of boundary information. However, the 2D CNN was utilized for segmenting 3D medical images, which led to the loss of spatial data, thereby affecting segmentation accuracy.

Khan *et al.* [26] presented a residual multi-scale UNet (RMS-UNet) to segment the liver and lesion effectively. Instead of using various kernel sizes, a multi-scale context layer with different dilation rates was applied to enhance the unique and valuable data from every layer. Residual blocks were included to compensate for training loss because of the increase in the amount of convolution layers. Batch normalization was applied in RMS-UNet to enhance learning without any loss of valuable information. However, RMS-UNet struggled with training stability due to complex interactions among residual and multi-scale components, which triggered convergence problems.

Kushnure *et al.* [27] suggested a lightweight multi-level multiscale network with a deep residual approach (LiM-Net) to segment the liver tumor using CT images. The computationally effective

pre-activated Res2Net with channel-wise attention (PARCA) was employed in the UNet for extracting multi-scale fine-grained features to enhance decoder competence. The network was optimized by utilizing a custom loss function that effectively managed class imbalances. Nonetheless, LiM-Net exhibited inaccurate segmentation because its lightweight design did not capture the complex tumor information effectively.

Ou *et al.* [28] implemented a ResTransUNet that integrated UNet and Transformer for liver tumor segmentation. The squeeze and excitation (SE) block were incorporated in UNet to capture more salient image features. A dual-path approach was employed in the encoding structure, where features were separately extracted utilizing both CNN and Transformer. An efficient feature enhancement unit was constructed for transferring the global extracted features by the Transformer to CNN, which enhanced its performance. Nevertheless, ResTransUNet had difficulties with training stability and convergence due to the integration of convolution and attention mechanisms, which struggled to effectively learn and optimize its parameters.

From the overall analysis, the existing methods are seen to have limitations as follows: over or under-segmentation errors, struggles in generalization ability, interpretability, and transparency. Moreover, it does not capture accurate boundaries in terms of size and depth. In order to address this issue, GGCN-CLR EfficientNet is proposed to accurately segment and classify liver tumors by using GCN and dynamic learning rate adjustments, which enable accurate delineation and tumor classification.

3. PROPOSED METHODOLOGY

In this research, GGCN-CLREN is proposed for segmenting and classifying liver tumors from CT images. LiTS17 and CHAOS are the two standard benchmark datasets used to determine the performance of the proposed approach. A median filter and data augmentation are used in the pre-processing phase to remove noise and increase the image size. Further, the GGCN is used to segment images while ResNext50 is applied to extract the features. Then, the golden sine gray wolf optimization (GSGWO) is established to select the extracted features. At last, CLREN classifies the liver tumors accurately. Figure 1 indicates a block diagram for the proposed approach.

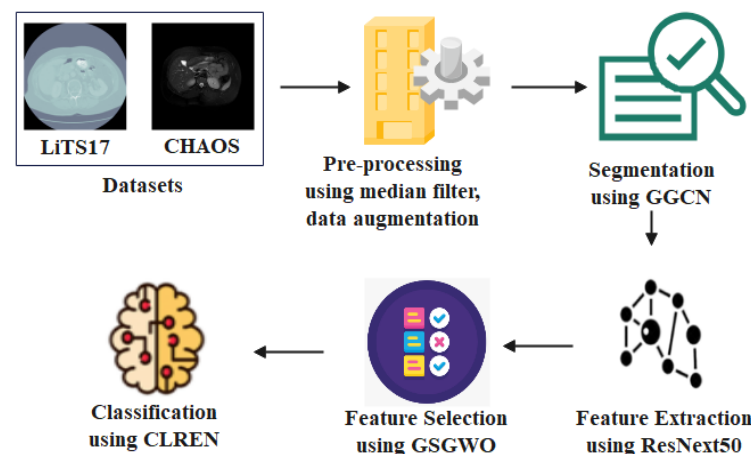


Figure 1. Block diagram for the proposed approach

3.1. Datasets

In this research, LiTS17 [29] and CHAOS [30] datasets are used for liver tumor segmentation. These two datasets are based on CT scans, which have many slice sizes, spacing, and thickness. A brief description of these datasets is explained as follows.

3.1.1. LiTS17

It contains a training set with 131 CT scans and a test set with 70 CT scans. Every CT contains varying slices, ranging from 42 to 1026, with 512×512-pixel resolution and a slice thickness ranging from 0.45 to 6.0 mm. The volume of the 131 CT scans is divided randomly into two parts: 30 cases for testing and

101 cases as training data. Figure 2 represents a sample image from the LiTS17 dataset, with Figure 2(a) representing the original image and Figure 2(b) representing the mask image.

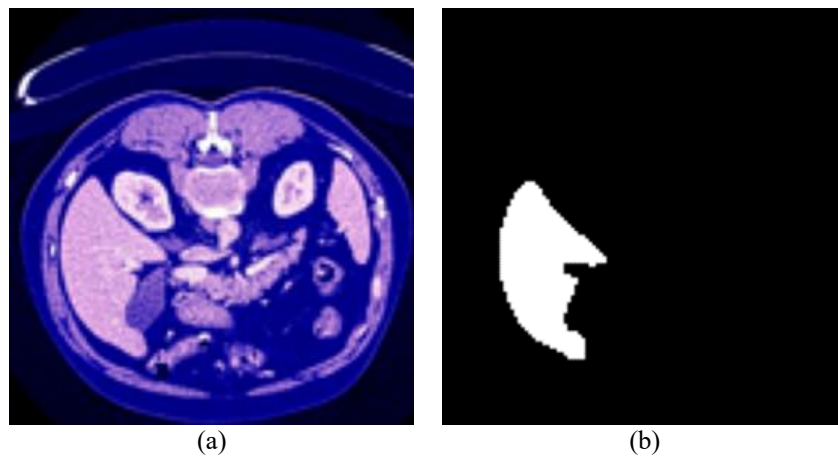


Figure 2. Sample images for LiTS17 dataset of (a) original image and (b) true mask

3.1.2. CHAOS

This dataset has CT images with varying slices, ranging from 42 to 1,026, with 512×512-pixel resolution, and slice thickness, including 6,407 sections from 40 patients. It is composed of 20 sets of unlabeled and 20 sets of labeled data. The 16 sets of CT images are selected randomly, with 416 sections for testing and 2,458 sections for training sets. The number of slices ranges from 81 to 266, with 512×512-pixel resolution and slice thickness ranging from 2.0 to 3.2 mm. Figure 3 indicates a sample image for the CHAOS dataset. Table 1 denotes the datasets description, and Figure 3 depicts the sample images from the CHAOS datasets in Figure 3(a) representing the original image and Figure 3(b) representing the true mask.

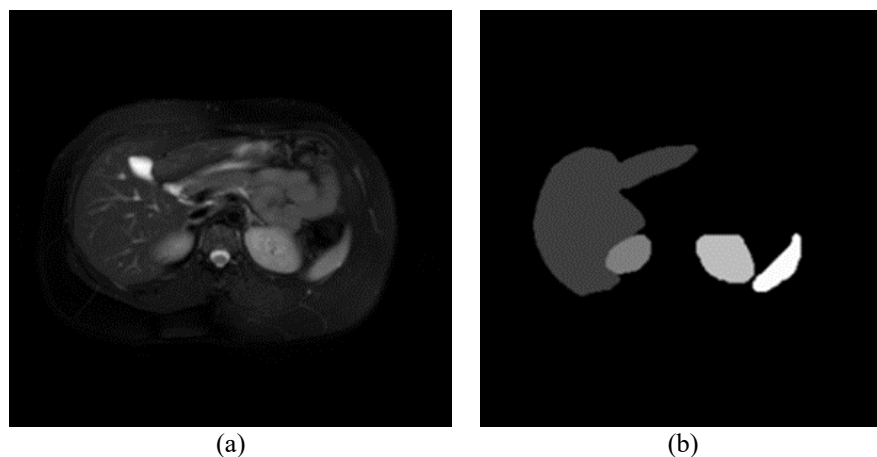


Figure 3. Sample images for CHAOS dataset of (a) original image and (b) true mask

Table 1. Dataset description

Dataset	Slice	Size of slice	Slice thickness (mm)	Slice spacing (mm)
LiTS17	42~1026	512×512	0.45~6.0	0.55~1.0
CHAOS	81~266	512×512	2.0~3.2	0.57~0.79

3.2. Pre-processing

The gathered input images are pre-processed utilizing two approaches: median filtering and data augmentation. These approaches enhance the image quality and increase the robustness and segmentation

performance of the model by generating more diverse training images in liver tumor, like padding, cropping, flipping, and random rotation. A detailed explanation of these methods is explained as follows.

3.2.1. Median filtering

A median filter [31] is a non-linear digital filter because it preserves the edges while removing impulse noise, such as salt and pepper noise, from the image of a liver tumor. This type of noise appears as dark pixels or isolated bright spots, which degrade the image quality. The median filter replaces each pixel with the median value from a local neighborhood, which effectively smoothes out noise-induced outliers while preserving significant image information and edges. Initially, the image's median value is acquired to read the pixel values, and then it is computed by choosing the middle value to modify the pixel's intensity value (x, y) . The process of median filtering is represented in (1). Here, ω represents the neighborhood pixel fixed at the $[m, n]$ location in the CT image, $y[m, n]$ denotes the output value of the filtered image, and $x[t, f]$ determines the input value in the original image. This process increases the image quality while preserving the significant edge information.

$$y[m, n] = \text{median} \{x[t, f]\}, (t, f) \in \omega \quad (1)$$

3.2.2. Data augmentation

Data augmentation assists in increasing the diversity of training data, which minimizes limited annotated images. Deep learning (DL) approaches require a significantly huge amount of labeled data for training. To solve this issue, data augmentation is performed to enhance the available data for training. It extends the data by utilizing various approaches like padding, cropping, random rotation, and horizontal flipping to create diverse variations of training images for DL method. Before efficiently deploying the DL approach, the data size is increased through synthetic augmentation for CT segmentation. It enhances model robustness by generating different transformations of the original images, which leads to better generalization and enhanced segmentation accuracy. Figures 4 and 5 represent sample augmented images for the LiTS17 and CHAOS datasets, which is demonstrated in: Figures 4(a) and 5(a) show the padding, Figures 4(b) and 5(b) show the cropping, Figures 4(c) and 5(c) show the random rotation, and Figures 4(d) and 5(d) show the horizontal flipping. The pre-processed data is fed as input to the segmentation process using GGCN.

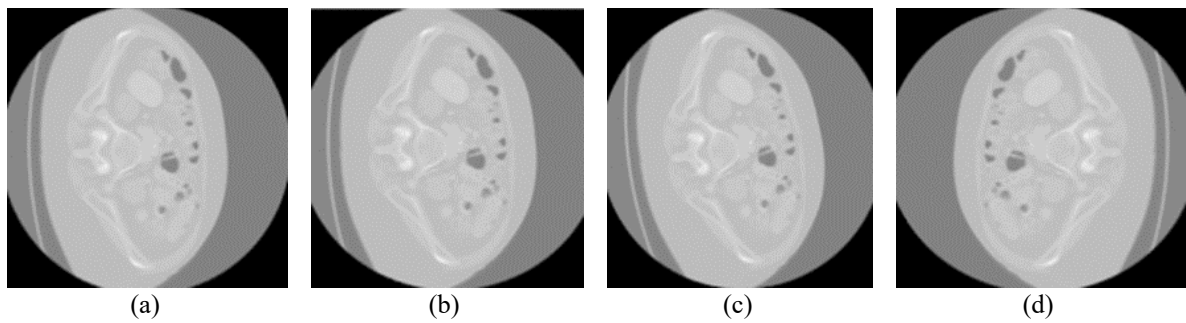


Figure 4. Sample augmented images for LiTS17 dataset of (a) padding, (b) cropping, (c) random rotation, and (d) horizontal flipping

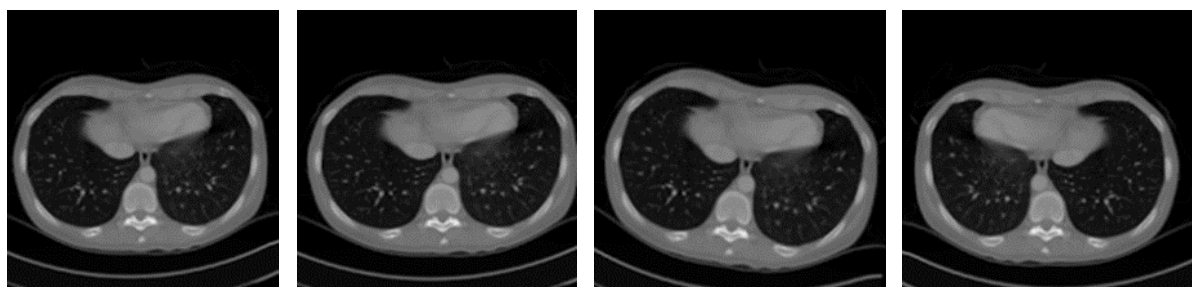


Figure 5. Sample augmented images for CHAOS dataset of (a) padding, (b) cropping, (c) random rotation, and (d) horizontal flipping

3.3. Segmentation

After pre-processing, GGCN is used to segment the liver tumor effectively. GGCN captures spatial relationships and dependencies effectively through a graph representation, which ensures model understanding of the various context tissues and organs. GGCN preserves structural data by representing the image as a graph and better models the relationships among regions or neighborhood pixels, which leads to more accurate segmentation. GGCN employs a coverage-aware grid query (CAGQ) by leveraging grid space efficiency and enhancing spatial coverage. For every point group generated by CAGQ, the GCA is employed for aggregating features from points of the node to the group center. Initially, a local graph $G(V, E)$ is constructed, where V is the group center, and K is the point of the node generated by CAGQ. Then, every node point is connected to the group center and develops node point features f_i to \tilde{f}_i . The GCA computes \tilde{f}_i and aggregates every feature as a center feature depending on the edge relation between the node and the center. The mathematical GCA module is expressed in (2) and (3). The \tilde{f}_i represents the node contribution, X_i denotes the xyz node location, \mathcal{M} determines the multi-layer perceptron (MLP), e shows the edge attention function, and A explains the aggregation function. The edge attention function is employed by using the center X_c and X_i node to model edge attention as a geometric relation function. Figure 6 represents the GGCN architecture.

$$\tilde{f}_{c,i} = e(X_i, f_i) * \mathcal{M}(f_i) \quad (2)$$

$$\tilde{f}_c = A(\{\tilde{f}_{c,i}\}, i \in 1, \dots, K) \quad (3)$$

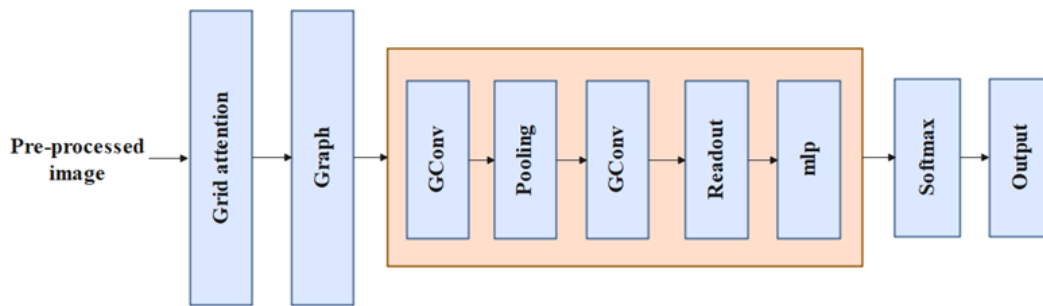


Figure 6. Architecture of GGCN

Moreover, the formulation disregards the underlying contribution of every node point from prior layers. The coverage weight is defined as the number of points aggregated to a node in prior layers. This value is calculated easily in CAGQ, and the coverage weight is a significant feature in computing edge attention. Semantic relation is another essential aspect of computing edge attention. The semantic relation is encoded by utilizing features of the group center f_c and the feature's node point f_i , which needs a center of the group to be chosen from the node points. The grid context pooling is established, which extracts the context features f_{cxt} by pooling from every context point in CAGQ that sufficiently covers the local graph's whole grid space. Grid context pooling determines the following benefits:

- f_{cxt} models the virtual group center features that enable the estimation of semantic relations among node points and centers.
- Even while the group center is selected at a physical point, f_{cxt} is significant in feature representation because it covers more points in a neighborhood instead of only graph points.
- In CAGQ, the context points are associated with their center voxel, and there are no extra query overhead points. In a local graph, f_{cxt} is shared among every edge computation, and the pooling is a lightweight operation requiring no learnable weight and less computational overhead. The edge attention function is formulated in (4).

$$e = \text{mlp}(\text{mlp}_{geo}(X_c, X_i, w_i), \text{mlp}_{sem}(f_{cxt}, f_i)) \quad (4)$$

Medical images vary significantly in pathology and anatomy. The GGCNs manage the irregular shapes of liver tumors by using graph structures, which leads to enhanced accuracy and robustness. Additionally, GGCN incorporates multi-scale data, which generates more data and accurate segmentation. Figure 7 indicates the segmented sample images, which are shown in Figure 7(a) representing the LiTS17

dataset and Figure 7(b) representing the CHAOS dataset. Then, the segmented input is fed into the feature extraction process using ResNext50.

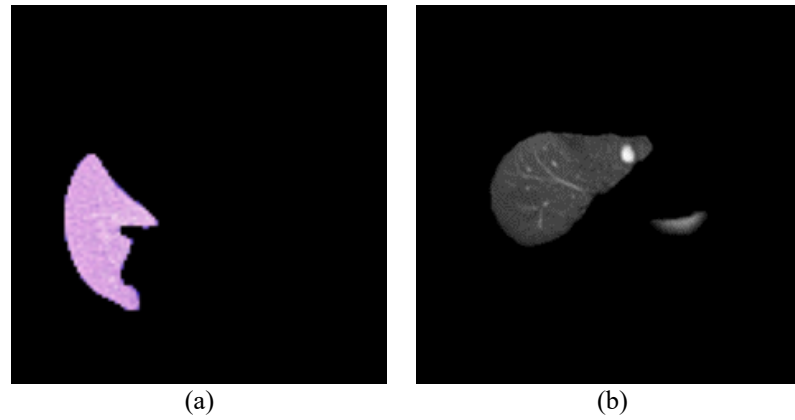


Figure 7. Sample for segmented images of (a) LiTS17 and (b) CHAOS

3.4. Feature extraction

After segmentation, ResNext50 [32] is performed to extract features effectively from liver tumors. ResNext50 enhances outcomes by using a highly modular architecture with grouped convolutions that improve feature extraction efficiency and model scalability. Its cardinality enhances the network's ability to learn diverse and rich features, which help in capturing the liver tumor's complex pattern. This model significantly minimizes computational demands while preserving information richness. The 1st convolutional layer utilizes a 7×7 convolutional kernel with a 2-stride, succeeded by 3×3 layers of max-pooling with a 2-stride. The second convolutional module has 3 kinds of convolutions: a 1×1 convolutional with 128 channels, a 3×3 convolutional with 128 channels, and a 1×1 convolutional with 256 channels. The third convolutional has a 1×1 convolutional with 256 channels, 3×3 convolutional with 256 channels split into 32 convolutional groups, and a 1×1 convolutional with 512 channels prepared in 4 groups. The fourth convolutional has a 1×1 convolutional kernel with 512 channels, a 3×3 convolutional with 512 channels split into 32 convolutional groups, and a 1×1 convolutional with 1,024 channels, repeated in 6 groups. The fifth convolutional has a 1×1 convolutional kernel with 1,024 channels, a 3×3 convolutional with 1,024 channels, which split into 32 convolutional groups, and a 1×1 convolutional with 2,048 channels, which are repeated in 3 groups. Then, the outcome is generated by using the average pooling layer and a fully connected (FC) layer. ResNext50 extracts 2,048 features effectively and increases the model's ability significantly, to capture diverse and intricate features within the segmented images. Also, ResNext50's depth and residual connections enable robust learning for more accurate and reliable tumor results.

3.5. Feature selection

After extracting features, the GSGWO is established to select the features from the LiTS17 and CHAOS datasets for liver tumors. The feature selection process is essential to increase the model's performance by minimizing dimensionality and focusing on the most appropriate features, which reduce overfitting and improve interpretability. GWO effectively explores and exploits the search space, leading to optimal feature subsets. This results in enhanced accuracy by choosing the most appropriate features from the extracted features. GWO [33] imitates the wolf-hunting approach for optimization. This approach splits the wolves into head wolf α , β , and δ , which helps the head wolf in hunting and is responsible for sentry, reconnaissance, along with another wolf ω . The wolves' hunting behavior is primarily split into three phases: encirclement, attack, and pursuit. In the encirclement stage, the GWO updates the position by utilizing (5) to (8).

$$X(t+1) = X_p(t) - A \cdot |C \cdot X_p(t) - X(t)| \quad (5)$$

$$A = 2a_1 \cdot r_1 - a_1 \quad (6)$$

$$C = 2r_2 \quad (7)$$

$$a_1 = 2 - 2t/t_{max} \quad (8)$$

Where X , X_p denote the gray wolf and prey wolf's position, A , C define the coefficient vectors, a_1 determines the convergence factor, r_1, r_2 determine the random number among $[0, 1]$, t indicates the present number of iterations, and t_{max} represents the maximum number of iterations. In the pursuit and attack stage, the GWO updates the position by (9) and (10). The X_1 , X_2 , and X_3 define the location update, which influences the factors of α , β , and δ wolves.

$$\begin{cases} X_1 = X_\alpha - A_1 \cdot |C_1 \cdot X_\alpha - X| \\ X_2 = X_\beta - A_2 \cdot |C_2 \cdot X_\beta - X| \\ X_3 = X_\delta - A_3 \cdot |C_3 \cdot X_\delta - X| \end{cases} \quad (9)$$

$$X(t+1) = (X_1 + X_2 + X_3)/3 \quad (10)$$

3.5.1. Golden sine algorithm

It is a meta-heuristic approach that transverses each point on a circle by the sine function and minimizes the search space by the golden coefficient, thereby enabling the model to achieve high search efficiency, jumping out of the local optima. The golden sine approach's position update equation is expressed in (11) and (12). The $X'(t+1)$ defines the model's convergence direction, r_1, r_2 denote the random numbers among $[0, 2\pi]$ and $[0, \pi]$. The s_1 and s_2 represent the golden algorithm coefficient, while τ determines the number of golden sections. The maximum accuracy is used as a fitness function, which is calculated in (13).

$$X'(t+1) = X(t+1) \cdot |\sin r_1| - r_2 \cdot \sin r_1 \cdot |s_1 \cdot X_1 - s_2 \cdot X(t+1)| \quad (11)$$

$$\begin{cases} s_1 = a \cdot \tau + b \cdot (1 - \tau) \\ s_2 = a \cdot (1 - \tau) + b \cdot \tau' \end{cases} \quad (12)$$

$$\text{Fitness Function} = \text{Maximum (Accuracy)} \quad (13)$$

The golden sine approach effectively performs secondary population convergence, optimizes the approach, and increases the algorithm's searchability. It selects 1,980 and 1,890 features for the LiTS17 and CHAOS datasets. The GSGWO provides an effective approach by incorporating local and global search abilities, ensuring accurate and optimal tumor delineation. After selecting the features, the GGCN-CLREN is performed for liver tumor classification.

3.6. Classification

Once the features are selected from the extracted features, EfficientNet classifies the liver tumor by leveraging a scalable architecture that balances the width, depth, and resolutions. It is a CNN model and scaling approach that applies compounded coefficients for scaling the dimensions evenly in the liver tumors. EfficientNet has 8 models between B0 and B7. As the number of models increases, the number of parameters does not rise significantly, but the accuracy decreases remarkably. The use of DL approach is to disclose more effective models with smaller approaches. EfficientNet achieves more efficient results by evenly scaling width, resolution, and depth when scaling down the approach. The main building block is an inverted MBConv bottleneck, which is generated in MobileNetV2 for EfficientNet. In MBConv, the blocks have a layer that is initially compressed and then enlarges the channel. Among bottlenecks, straight connections associated with fewer channels compared to the expanded layers are employed. Furthermore, this structure has in-depth separable convolutions that reduce the calculation by a K^2 factor, where the K kernel size denotes the height and width of the convolution window. The compound coefficient θ is utilized for scaling evenly, which is expressed in (14).

$$\begin{aligned} \text{Width: } W &= \mathcal{X}^\zeta \\ \text{Depth: } D &= \beta^\zeta \\ \text{Resolution: } R &= \delta^\zeta \\ \beta \geq 1, \mathcal{X} \geq 1, \delta \geq 1 \end{aligned} \quad (14)$$

Where $\beta, \mathcal{X}, \delta$ denotes a constant that is calculated by grid search, and θ is determined as a user-defined coefficient that handles the available resources to scale the model. The floating-point operations per second (FLOPS) are proportional to D, W^2, R^2 . Computing costs in convolution networks are greater owing to the

convolution operation, while scaling convolutional networks increases the FLOPS network by approximately $(\beta, \mathcal{X}^2, \delta^2)^\theta (\beta, \mathcal{X}^2, \delta^2)^\theta$. The compound scaling approach scales this model in 2 stages:

- Stage 1: considering that there are more than two available resources, a grid search is performed with $\theta = 1$, and ideal values are established from β, \mathcal{X} , and δ .
- Stage 2: the obtained β, \mathcal{X} , and δ values are determined as constants, and the standard network is scaled up to obtain EfficientNet-B1 to B7 with varying θ values.

The rectified linear unit (ReLU) is used as an activation function for the liver tumors. CLR is used to acquire the optimal learning rate in liver tumors by fluctuating between the maximum learning rate of 10 and a base learning rate of 1e-8. With a step size of 50 and a cycle length of 100, the CLR adjusts the learning rate within this range over 100 iterations by utilizing a batch size of 32. The overfitting issue is solved by using CLR during training, allowing the model to explore a wider range of learning rates. The max and base learning rates determine a range boundary where the rate of learning is fluctuated. These dynamic adjustments enable the model to train more effectively by rapid convergence. Incorporating CLR and EfficientNet enhances training stability, optimizes learning rate for better performance, and obtains a high accuracy with fewer resources, which renders this approach highly effective for the classification of liver tumor.

4. EXPERIMENTAL RESULTS

The results and discussion of the performance analysis are presented in this section. The proposed approach is evaluated using software tools: Anaconda Navigator 3.5.2.0 (64-bit), Python 3.10.12 with Windows 10 operating systems, i5 Intel-core, and 8 GB RAM. The frameworks and libraries used here are Transformers, Tensorflow, Keras, Sklearn frameworks, and Matplotlib library to plot. The performance metrics utilized in this research are dice similarity coefficient (DSC), accuracy, recall, precision, volumetric overlapping error (VOE), and relative volume difference (RVD), which are expressed in (15) to (21). The TP , FN , TN , and FP represent true positive, false negative, true negative, and false positive, and $|X|$ and $|Y|$ indicate the volumes of X and Y , respectively.

$$Accuracy = \frac{TP+TN}{TP+TN+FP+FN} \quad (15)$$

$$Precision = \frac{TP}{TP+FP} \quad (16)$$

$$Recall = \frac{TP}{TP+FN} \quad (17)$$

$$F1 - Score = \frac{2TP}{2TP+FP+FN} \quad (18)$$

$$Dice(X, Y) = \frac{2|X \cap Y|}{|X| + |Y|} \quad (19)$$

$$RVD(X, Y) = \frac{|Y| - |X|}{|X|} \quad (20)$$

$$VOE(X, Y) = 1 - \frac{2|X \cap Y|}{|X| + |Y|} \quad (21)$$

4.1. Performance analysis

Table 2 presents the performance analysis of segmentation methods using the LiTS17 and CHAOS datasets. The existing approaches of UNet, Superpixel segmentation, and GCN are compared with the GGCN approach. When compared to these existing approaches, GGCN achieves a better DSC of 98.50% and 97.95% using the LiTS17 and CHAOS datasets due to it effectively integrating the spatial structure of grid data with GCN, which enables more accurate modeling of complex tumor shapes and spatial relationships. Also, it employs both global and local contexts, which increase its ability to capture complex boundaries and variations.

Table 3 denotes a performance analysis of feature selection methods for LiTS17 and CHAOS datasets. Particle swarm optimization (PSO), ant colony optimization (ACO), and GWO are compared with GSGWO, which achieves a better accuracy of 99.80% and 99.96%. As the proposed approach enhances exploitation and exploration balance by including the golden sine strategy, the convergence speed is improved, alongside avoiding the local optima issue. This approach integrates the strengths of the sine cosine

mechanism with the adaptive hunting behavior of gray wolves, which leads to more accurate and effective optimization.

Table 2. Performance analysis of segmentation methods

Dataset	Methods	DSC (%)	VOE (%)	RVD (%)
LiTS17	Unet	95.23	5.06	1.25
	Superpixel segmentation	91.25	5.85	2.14
	GCN	90.56	6.54	2.77
	GGCN	98.50	4.33	0.11
CHAOS	Unet	87.69	6.83	2.55
	Superpixel segmentation	92.58	5.69	1.27
	GCN	88.45	6.12	2.04
	GGCN	97.95	3.78	0.13

Table 3. Performance analysis of feature selection methods

Dataset	Methods	Accuracy (%)	Precision (%)	Recall (%)	F1-score (%)
LiTS17	PSO	82.53	81.00	80.00	80.49
	ACO	89.50	89.00	87.00	87.98
	GWO	78.38	79.00	78.00	78.49
	GSGWO	99.80	99.52	99.50	99.51
CHAOS	PSO	85.42	85.00	84.00	84.49
	ACO	70.69	72.00	70.00	70.98
	GWO	79.53	79.00	78.00	78.89
	GSGWO	99.96	99.89	99.90	99.89

Table 4 shows a performance analysis of classification with default features. The CLREN exhibits superior accuracy of 95.35% and 96.24% when compared to fully convolution networks (FCN), visual geometry group (VGG), and InceptionV3, as the proposed approach combines EfficientNet with CLR that adjusts dynamic learning rates to escape local minima and increase convergence. This approach enhances generalization abilities, which leads to superior performance in classifying liver tumors.

Table 4. Performance analysis of classification with default features

Dataset	Methods	Accuracy (%)	Precision (%)	Recall (%)	F1-score (%)
LiTS17	FCN	88.26	85.37	84.06	84.70
	VGG	62.85	65.12	69.01	67.00
	InceptionV3	74.25	72.06	74.58	73.29
	CLREN	95.35	94.05	92.14	93.08
CHAOS	FCN	86.64	85.14	85.58	85.35
	VGG	89.25	85.24	86.32	85.77
	InceptionV3	70.47	69.21	70.43	69.81
	CLREN	96.24	95.14	93.28	94.20

Table 5 determines the performance analysis of classification with optimized features. When compared to FCN, VGG, and InceptionV3, CLREN achieves a better accuracy of 99.80% and 99.96% using the LiTS17 and CHAOS datasets, as it employs the compound scaling method of EfficientNet, which optimizes the depth, resolution, and width for an improved performance. Also, CLR increases the training process by adjusting dynamic learning rates, which results in effective learning and enhanced accuracy.

Table 5. Performance analysis of classification with optimized features

Dataset	Methods	Accuracy (%)	Precision (%)	Recall (%)	F1-score (%)
LiTS17	FCN	98.05	98.00	98.00	98
	VGG	75.5	75.00	74.50	74.74
	InceptionV3	80.13	80.00	80.00	80
	CLREN	99.80	99.52	99.50	99.51
CHAOS	FCN	97.90	97.00	97.00	97
	VGG	98.60	98.10	98.00	98.04
	InceptionV3	73.00	73.00	73.00	73
	CLREN	99.96	99.89	99.90	99.89

Table 6 demonstrates the performance of K-fold validation. When $K=5$, fold validation provides a good balance among bias and variance. With fewer folds, $K=3$, the training sets are larger but the validation is smaller, resulting in higher variance in validation outcomes. With $K=7$ folds, the training sets are smaller, leading to high bias. $K=5$ provides a balance and produces more stable and reliable performance.

Figure 8 illustrates the performance analysis of epoch vs. accuracy for CLREN, where Figure 8(a) shows results of LITS17 and Figure 8(b) displays results of CHAOS datasets. The blue line indicates training accuracy, which increases gradually, after which the model learns from the training data. The orange line represents validation accuracy that enhances and levels off, which performs well on new data. Both accuracies increase rapidly, which indicate that the model offers an improved performance.

Figure 9 determines a performance analysis of epoch vs. loss, where Figure 9(a) shows results of LITS17 and Figure 9(b) displays results of CHAOS datasets using proposed CLREN. The blue line indicates the training loss, while the orange line shows validation loss over 10 epochs. Both losses decrease rapidly, indicating that the model learns and improves its performance on both training and validation data. The validation loss is slower than the training loss, which implies that the model generalizes well on unseen data.

Table 6. Performance analysis of K-fold validation

Dataset	K-fold	Accuracy (%)	Precision (%)	Recall (%)	F1-score (%)
LITS17	3.00	82.54	81.56	79.23	80.37
	5.00	99.80	99.52	99.50	99.51
	7.00	85.27	84.57	81.05	82.77
	9.00	89.39	88.26	86.56	87.40
CHAOS	3.00	84.21	83.74	83.43	83.58
	5.00	99.96	99.89	99.90	99.89
	7.00	86.87	85.34	83.47	84.39
	9.00	91.34	90.23	89.15	89.68

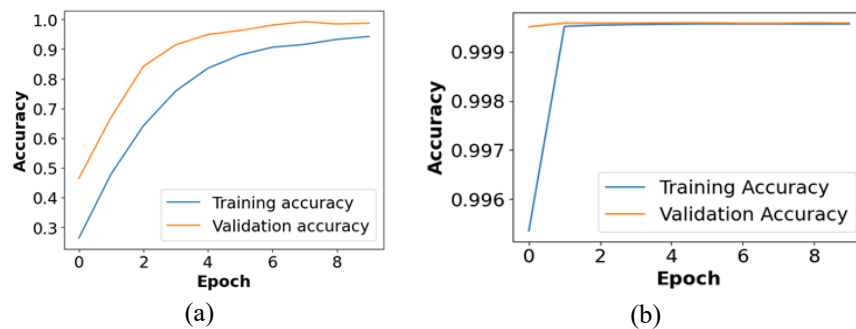


Figure 8. Performance analysis of epoch vs. accuracy of (a) LiTS17 and (b) CHAOS

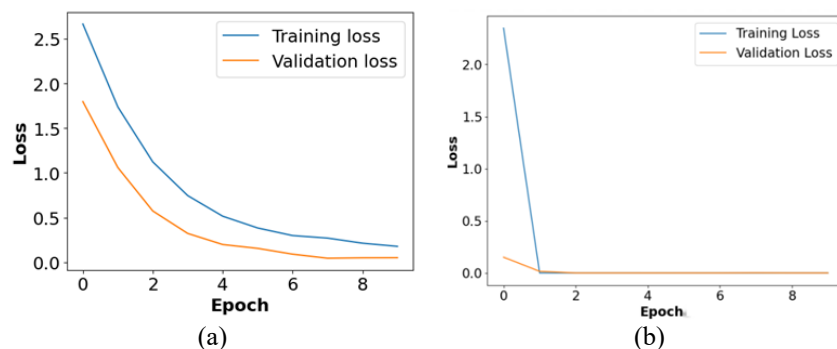


Figure 9. Performance analysis of epoch vs. loss of (a) LiTS17 (b) CHAOS

4.2. Comparative analysis

Table 7 represents a comparative analysis of existing methods using the LiTS17 and CHAOS datasets. When compared to the existing methods like DS-AI-CRF [19], APESTNet [21], IPNN-BO [22], and

RMS-UNet [26], the proposed GGCN-CLREN achieves a better accuracy of 99.80% and 99.96% for both datasets. The proposed approach employs an advanced GCN to effectively capture spatial relationships and integrates it with CLREN to dynamically optimize learning rates, so as to augment the model's performance in liver tumors.

Table 7. Comparative analysis of existing methods

Methods	Dataset	Accuracy (%)	Precision (%)	Recall (%)	Dice (%)	VOE (%)	RVD (%)
DS-AI-CRF [19]	LiTS17	N/A	N/A	N/A	97.62	4.64	0.42
APESTNet [21]		95.62	98.32	94.62	N/A	N/A	N/A
IPNN-BO [22]		99.25	N/A	98.63	N/A	N/A	N/A
Proposed GGCN-CLREN		99.80	99.52	99.50	98.50	4.33	0.11
AIM-UNet [23]	CHAOS	99.75	99.69	96.39	97.86	N/A	N/A
RMS-UNet [26]		N/A	N/A	N/A	95.49	10.87	1.2
Proposed GGCN-CLREN		99.96	99.89	99.90	97.95	3.78	0.13

4.3. Discussion

The advantages of the proposed method and the limitations of existing methods are discussed in this section. The existing method limitations, like DS-AI-CRF [19], face over or under-segmentation errors when level tumors are situated at the boundaries due to their complex spatial relationships and variations. APESTNet [21] faces challenges in adapting to different tumor appearances and anatomical variations due to the capturing of subtle features specific to different tumor types. IPNN-BO [22] struggles with intricate interactions among tumor characteristics due to complex and non-linear relationships among various features. AIM-UNet [23] suffers from increased memory usage and potential overfitting due to a large number of parameters introduced by the Inception modules, which impact the model's performance. RMS-UNet [26] faces challenges in training stability due to complex interactions among the residual and multi-scale components, which lead to convergence problems. The proposed GGCN-CLREN overcomes these existing method limitations. This approach effectively captures spatial dependencies and complex structures within images by using GCN, which improves segmentation accuracy through modeling complex tissue patterns and boundaries. Also, the CLREN adjusts learning rates dynamically, while also improving training efficiency and convergence speed, outperforming traditional methods in terms of classification performance.

5. CONCLUSION

In this research, the GGCN-CLREN is proposed to accurately segment and classify liver tumors. This approach assists EfficientNet in effectively learning complex features, which in turn improve classification accuracy and robustness. CLR obtains an optimal learning rate in liver tumors by fluctuating between the maximum learning rate and a base learning rate with the step size. Further, the GGCN conserves the structural data by representing the image as a graph and modeling the relationships between the neighborhood pixels or regions, giving rise to a more accurate segmentation. ResNext50 extracts features effectively by using grouped convolutions that improve feature extraction efficiency and model scalability. GSGWO incorporates both local and global search abilities, and ensures an accurate and optimal tumor delineation. By performing all these processes, GGCN-CLREN achieves a commendable accuracy of 99.80% and 99.96%, as opposed to the existing techniques, APESTNet and AIM-UNet, respectively. In the future, a hybrid method will be considered to further improve the model's outcomes.

FUNDING INFORMATION

Authors state no funding involved.

AUTHOR CONTRIBUTIONS STATEMENT

This journal uses the Contributor Roles Taxonomy (CRediT) to recognize individual author contributions, reduce authorship disputes, and facilitate collaboration.

Name of Author	C	M	So	Va	Fo	I	R	D	O	E	Vi	Su	P	Fu
Sangi Narasimhulu	✓	✓	✓	✓	✓	✓		✓	✓	✓			✓	✓
Ch D V Subba Rao		✓				✓	✓	✓	✓	✓	✓	✓		

C : Conceptualization	I : Investigation	Vi : Visualization
M : Methodology	R : Resources	Su : Supervision
So : Software	D : Data Curation	P : Project administration
Va : Validation	O : Writing - Original Draft	Fu : Funding acquisition
Fo : Formal analysis	E : Writing - Review & Editing	

CONFLICT OF INTEREST STATEMENT

The authors declare no conflict of interest.

DATA AVAILABILITY

The data that support the findings of this study are openly available in [LiTS17] at <https://www.kaggle.com/datasets/andrewmvd/liver-tumor-segmentation-part-2> and [CHAOS] at <https://www.kaggle.com/datasets/anhoangvo/chaos-t1-and-t2>.




REFERENCES

- [1] A. Kalsoom, M. Maqsood, S. Yasmin, M. Bukhari, Z. Shin, and S. Rho, "A computer-aided diagnostic system for liver tumor detection using modified U-Net architecture," *The Journal of Supercomputing*, vol. 78, no. 7, pp. 9668–9690, May 2022, doi: 10.1007/s11227-021-04266-6.
- [2] S. Huang *et al.*, "Sd-net: a semi-supervised double-cooperative network for liver segmentation from computed tomography (CT) images," *Journal of Cancer Research and Clinical Oncology*, vol. 150, no. 2, Feb. 2024, doi: 10.1007/s00432-023-05564-7.
- [3] Y. You, Z. Bai, Y. Zhang, and Z. Li, "Contour-induced parallel graph reasoning for liver tumor segmentation," *Biomedical Signal Processing and Control*, vol. 92, Jun. 2024, doi: 10.1016/j.bspc.2024.106111.
- [4] K. Hettihewa, T. Kobchaisawat, N. Tanpowpong, and T. H. Chalidabhongse, "MANet: a multi-attention network for automatic liver tumor segmentation in computed tomography (CT) imaging," *Scientific Reports*, vol. 13, no. 1, Nov. 2023, doi: 10.1038/s41598-023-46580-4.
- [5] J. Sun, B. Wang, X. Wu, C. Tang, S. Wang, and Y. Zhang, "MAPFUNet: multi-attention perception-fusion U-Net for liver tumor segmentation," *Journal of Bionic Engineering*, vol. 21, no. 5, pp. 2515–2539, Sep. 2024, doi: 10.1007/s42235-024-00562-y.
- [6] U. Hameed, M. U. Rehman, A. Rehman, R. Damaševičius, A. Sattar, and T. Saba, "A deep learning approach for liver cancer detection in CT scans," *Computer Methods in Biomechanics and Biomedical Engineering: Imaging & Visualization*, vol. 11, no. 7, Jan. 2024, doi: 10.1080/21681163.2023.2280558.
- [7] L. Sun *et al.*, "A teacher-student framework for liver and tumor segmentation under mixed supervision from abdominal CT scans," *Neural Computing and Applications*, vol. 34, no. 19, pp. 16547–16561, Oct. 2022, doi: 10.1007/s00521-022-07240-2.
- [8] J. Kaur and P. Kaur, "PSO-PSP-NET + InceptionV3: an optimized hyper-parameter tuned computer-aided diagnostic model for liver tumor detection using CT scan slices," *Biomedical Signal Processing and Control*, vol. 95, Sep. 2024, doi: 10.1016/j.bspc.2024.106442.
- [9] M. Y. Ansari *et al.*, "Practical utility of liver segmentation methods in clinical surgeries and interventions," *BMC Medical Imaging*, vol. 22, no. 1, May 2022, doi: 10.1186/s12880-022-00825-2.
- [10] A. Biswas, S. P. Maity, R. Banik, P. Bhattacharya, and J. Debbarna, "GAN-driven liver tumor segmentation: enhancing accuracy in biomedical imaging," *SN Computer Science*, vol. 5, no. 5, Jun. 2024, doi: 10.1007/s42979-024-02991-2.
- [11] R. Zheng *et al.*, "Automatic liver tumor segmentation on dynamic contrast enhanced MRI using 4D information: deep learning model based on 3D convolution and convolutional LSTM," *IEEE Transactions on Medical Imaging*, vol. 41, no. 10, pp. 2965–2976, Oct. 2022, doi: 10.1109/TMI.2022.3175461.
- [12] U. Bhimavarapu, "Automatic liver tumor detection and classification using the hyper tangent fuzzy C-means and improved fuzzy SVM," *Multimedia Tools and Applications*, vol. 83, no. 15, pp. 46201–46220, Oct. 2023, doi: 10.1007/s11042-023-17430-2.
- [13] Y. Chen *et al.*, "Efficient two-step liver and tumour segmentation on abdominal CT via deep learning and a conditional random field," *Computers in Biology and Medicine*, vol. 150, Nov. 2022, doi: 10.1016/j.compbiomed.2022.106076.
- [14] Z. Wang, J. Zhu, S. Fu, and Y. Ye, "Context fusion network with multi-scale-aware skip connection and twin-split attention for liver tumor segmentation," *Medical & Biological Engineering & Computing*, vol. 61, no. 12, pp. 3167–3180, Dec. 2023, doi: 10.1007/s11517-023-02876-1.
- [15] X. Tang *et al.*, "Segmentation-guided multi-modal registration of liver images for dose estimation in SIRT," *European Journal of Nuclear Medicine and Molecular Imaging Physics*, vol. 9, no. 1, Dec. 2022, doi: 10.1186/s40658-022-00432-8.
- [16] J. Wang, X. Zhang, P. Lv, H. Wang, and Y. Cheng, "Automatic liver segmentation using EfficientNet and attention-based residual U-Net in CT," *Journal of Digital Imaging*, vol. 35, no. 6, pp. 1479–1493, Dec. 2022, doi: 10.1007/s10278-022-00668-x.
- [17] S. Di, Y. Zhao, M. Liao, Z. Yang, and Y. Zeng, "Automatic liver tumor segmentation from CT images using hierarchical iterative superpixels and local statistical features," *Expert Systems with Applications*, vol. 203, 2022, doi: 10.1016/j.eswa.2022.117347.
- [18] R. V. Manjunath and K. Kwadiki, "Automatic liver and tumour segmentation from CT images using deep learning algorithm," *Results in Control and Optimization*, vol. 6, Mar. 2022, doi: 10.1016/j.rico.2021.100087.
- [19] P. Lv, J. Wang, X. Zhang, and C. Shi, "Deep supervision and atrous inception-based U-Net combining CRF for automatic liver segmentation from CT," *Scientific Reports*, vol. 12, no. 1, Oct. 2022, doi: 10.1038/s41598-022-21562-0.
- [20] D. Popescu, A. Stanculescu, M. D. Pomohaci, and L. Ichim, "Decision support system for liver lesion segmentation based on advanced convolutional neural network architectures," *Bioengineering*, vol. 9, no. 9, 2022, doi: 10.3390/bioengineering9090467.
- [21] P. K. Balasubramanian, W.-C. Lai, G. H. Seng, K. C., and J. Selvaraj, "APESTNet with mask R-CNN for liver tumor segmentation and classification," *Cancers*, vol. 15, no. 2, Jan. 2023, doi: 10.3390/cancers15020330.
- [22] S. Kolli, B. R. Parvathala, and A. V. P. Krishna, "A novel liver tumor classification using improved probabilistic neural networks with Bayesian optimization," *e-Prime - Advances in Electrical Engineering, Electronics and Energy*, vol. 8, Jun. 2024, doi: 10.1016/j.prime.2024.100514.




- [23] F. Özcan, O. Uçan, S. Karaçam, and D. Tunçman, "Fully automatic liver and tumor segmentation from CT image using an AIM-UNet," *Bioengineering*, vol. 10, no. 2, Feb. 2023, doi: 10.3390/bioengineering10020215.
- [24] Z. Xia, M. Liao, S. Di, Y. Zhao, W. Liang, and N. N. Xiong, "Automatic liver segmentation from CT volumes based on multi-view information fusion and condition random fields," *Optics & Laser Technology*, vol. 179, Dec. 2024, doi: 10.1016/j.optlastec.2024.111298.
- [25] X. Xie, X. Pan, F. Shao, W. Zhang, and J. An, "MCI-Net: multi-scale context integrated network for liver CT image segmentation," *Computers and Electrical Engineering*, vol. 101, Jul. 2022, doi: 10.1016/j.compeleceng.2022.108085.
- [26] R. A. Khan, Y. Luo, and F.-X. Wu, "RMS-UNet: residual multi-scale UNet for liver and lesion segmentation," *Artificial Intelligence in Medicine*, vol. 124, Feb. 2022, doi: 10.1016/j.artmed.2021.102231.
- [27] D. T. Kushnure, S. Tyagi, and S. N. Talbar, "LiM-Net: lightweight multi-level multiscale network with deep residual learning for automatic liver segmentation in CT images," *Biomedical Signal Processing and Control*, vol. 80, Feb. 2023, doi: 10.1016/j.bspc.2022.104305.
- [28] J. Ou, L. Jiang, T. Bai, P. Zhan, R. Liu, and H. Xiao, "ResTransUnet: an effective network combined with transformer and U-Net for liver segmentation in CT scans," *Computers in Biology and Medicine*, vol. 177, Jul. 2024, doi: 10.1016/j.compbio.2024.108625.
- [29] L. Tinglan, Q. Jun, Q. Guihe, S. Weili, and Z. Wentao, "Liver segmentation network based on detail enhancement and multi-scale feature fusion," *Scientific Reports*, vol. 15, no. 1, Jan. 2025, doi: 10.1038/s41598-024-78917-y.
- [30] M. Reyad, A. M. Sarhan, and M. Arafa, "Architecture optimization for hybrid deep residual networks in liver tumor segmentation using a GA," *International Journal of Computational Intelligence Systems*, vol. 17, no. 1, 2024, doi: 10.1007/s44196-024-00542-4.
- [31] H. Habib, R. Amin, B. Ahmed, and A. Hannan, "Hybrid algorithms for brain tumor segmentation, classification and feature extraction," *Journal of Ambient Intelligence and Humanized Computing*, vol. 13, no. 5, pp. 2763–2784, May 2022, doi: 10.1007/s12652-021-03544-8.
- [32] Q. Liu, M. Jiang, J. Wang, D. Wang, and Y. Tao, "The rapid determination of three toxic ginkgolic acids in the decolorized process of Ginkgo Ketone Ester based on Raman spectroscopy and ResNeXt50 deep neural network," *Chemosensors*, vol. 12, no. 1, Dec. 2023, doi: 10.3390/chemosensors12010006.
- [33] D. Zhao, G. Cai, Y. Wang, and X. Li, "Path planning of obstacle-crossing robot based on golden sine grey wolf optimizer," *Applied Sciences*, vol. 14, no. 3, Jan. 2024, doi: 10.3390/app14031129.

BIOGRAPHIES OF AUTHORS



Sangi Narasimhulu    received M.Tech. (CSE) from JNTU Anantapur, Ananthapuramu in the year 2013. He has 7 years of teaching experience. Currently, he is pursuing his Ph.D. in the Department of Computer Science and Engineering, Sri Venkateswara University College of Engineering, Tirupati, Andhra Pradesh, India. His areas of interest are software engineering, artificial intelligence, machine learning, and deep learning. He can be contacted at email: narasimhulu.sangi@gmail.com.



Ch D V Subba Rao    has been working as a faculty member in the Department of Computer Science and Engineering, Sri Venkateswara University College of Engineering since 1992, and as Professor since 2009. His areas of interest include distributed systems, peer to peer systems, wireless networks, and advanced computing. He published 78 papers in international/national journals. Some of his publications appear in IEEE, ACM, Elsevier, and Springer digital libraries. He guided 41 M.Tech. theses and 7 Ph.D. theses. At present, he is supervising the work of 8 Ph.D. scholars. He visited Austria, Hong-Kong, Netherlands, Belgium, Thailand, and Germany, and chaired the sessions of International Conferences, viz. IEEE, IAENG, and IASTED. He is serving as Member, Board of Studies in CSE/IT of Bharatiya University/Coimbatore, DU/Kuppam, RGUKT/Nuzvid, SVU/Tirupati, and number of autonomous Engineering Colleges. He served as Head, Department of Computer Science and Engineering (for two terms), Officer-in-Charge, Computer Centre of Sri Venkateswara University College of Engineering, and Coordinator/MSIT Program. He worked as a faculty member at NIT/Warangal in 1992. He can be contacted at email: chdvsrao@gmail.com.